9TH INTERNATIONAL SYMPOSIUM ON PARTICLE IMAGE VELOCIMETRY - PIV11
Kobe, Japan, July 21-23, 2011

Investigation of the Wake of Low Aspect Ratio Cylinders by Tomographic PIV

B. Heine[1], D. Schanz[2], A. Schröder[3], U. Dierksheide[4], M. Raffel[5]

[1,2,3,5]Institute of Aerodynamics and Flow Technology, DLR Göttingen, 37073 Göttingen, Germany
benjamin.heine@dlr.de

[4]LaVsion GmbH, 37073 Göttingen, Germany

ABSTRACT

The wakes of wall mounted circular cylinders of very low aspect ratio have been investigated in a wind tunnel. Besides planar PIV, also high resolution tomographic PIV was used to capture the flow phenomena downstream of the cylinder. By changing the velocity U_∞ and the cylinder height h at a constant aspect ratio $\Lambda = h/D$, a wide database of different flow conditions was obtained. The resulting relative height of the boundary layer thickness δ was $0.6 \leq h/\delta \leq 2.5$, while the Reynolds number based on the length l between leading edge and cylinder centre Re_l was $57,000 \leq Re_l \leq 188,000$. A pair of counter-rotating vortices was found in the wake of the cylinder. The rotation sense is such, that in the center of the wake a positive vertical velocity component results. Also horseshoe vortices were found next to these trailing vortices. The relative height of the incoming boundary layer has a large impact on the development, strength and dissipation of the vortex system.

1. INTRODUCTION

The phenomenon of dynamic stall is considered a limiting factor for a helicopter's forward flight performance but also reduces the efficiency of e.g. wind turbines [13, 2]. In most cases it induces an abrupt decay and fluctuations of the aerodynamic loads, resulting in high structural loads, drag, noise and control forces. Therefore numerous active and passive devices have been investigated in order to reduce the negative impact of the dynamic stall vortex. Rotor systems have to face high centrifugal forces, hence a simple, passive device is desirable.

Geissler *et al.* [5] developed a very simple device, called LEVoGs (Leading Edge Vortex Generators) that improve the aerodynamic performance of a wing under dynamic stall conditions significantly [11]. The passive flow control device consists of a row of small circular cylinders with a low aspect ratio. The diameter of 2% chord and aspect ratio of 0.09 of the LEVoGs was found during a parameter study by Mai *et al.* [11].

Nevertheless, the principle of operation of these leading edge devices is not clear, but the knowledge of the aerodynamic behavior is essential in order to optimize such devices and adapt them to other applications. Previous studies by Heine *et al.* [7] confirm the positive effects and visualize the global impact of these low aspect ratio cylinders. A further investigation on the impact of LEVoGs on the flow around the simple geometry of an infinite circular cylinder aimed to get a closer view on the principle of operation of the LEVoGs [8]. However, it was found that it is a challenging task to investigate the aerodynamic phenomena due to the unsteady behavior and small scale.

Therefore an even more fundamental approach was selected where the circular cylinder shape of the LEVoGs was scaled up and mounted onto a flat plate. While the flow around an infinite circular cylinder has been investigated by many researchers, the number of publications about the cylinder flow with low aspect ratio is limited.

It was found that for aspect ratios below a certain value the characteristic asymetric separation of the von Kármán vortex shedding is suppressed from base to tip and replaced by symmetric arc vortex shedding. Here, also the ratio between the boundary layer thickness and cylinder has a strong influence. Okamoto *et al.* [14] found this to be below $1 \leq \Lambda \leq 2$ ($h/\delta = 9.1$), Lee *at al.* [10] for $\Lambda = 3$ ($h/\delta = 6.66$) and Kawamura *at al.* [9] for $\Lambda = 4$ ($h/\delta = 4$). In addition, the characteristic pair of tip vortices that induce a downwash in the wake of the cylinder are suppressed [15, 4]. Other researchers have reported an absence of a peak in the power spectrum for very short cylinders [17], also indicating a complete absence of regular Karman vortex shedding.

Pattenden *et al.* [16] provide a comprehensive overview of the flow around a finite cylinder of aspect ratio 1. By means of planar PIV, surface pressure measurements and flow visualization they were able to reconstruct the flow field including the symmetric vortex system. This system consists of three dominant vortices: A horseshoe vortex that bends around the leading edge of the cylinder, an arch vortex in the direct wake and the trailing vortices further downstream.

Gregory *et al.* [6] investigated circular surface bumps with aspect ratios between 0.06 and 1 by means of oil flow and smoke visualization. However, to the knowledge of the authors, there are no detailed publications about the flow around a cylinders with very low aspect ratio.

The present paper deals with the flow around a circular cylinder with the aspect ratio of 0.09. Measurements at several velocities and cylinder heights resulted in a database of different Reynolds numbers Re_l and relative heights h/δ. The flow field was analyzed using planar PIV and high resolution tomographic PIV. The larger scale planar PIV setup through the symmetry plane of the configuration was used to capture global parameters including the incoming boundary layer height, velocity fluctuations etc. For the tomographic PIV, the light volume was placed directly behind the cylinder and illuminated seeding particles were recorded by four cameras.

2. EXPERIMENTAL SETUP

A flat glass plate with an elliptical leading edge (ratio 3:1) has been placed into the closed-circuit low-speed wind tunnel (1MG) at the DLR in Göttingen. It has an open test section with dimensions 1.0 m x 0.7 m x 1.4 m (W x H x L). The tunnel was operated at velocities from U_∞ = 3.4 - 23.5 m/s where the turbulence level is Tu $\approx$ 0.15 %. Two configurations were investigated: One with 12:1 and one with 6:1 upscaled LEVoGs mounted onto the flat plate with a spacing of $D/s = 0.3$ according to the suggested application on a rotorblade [5]. Since no typical cylinder flow with von Kármán vortex shedding was present, the Reynolds number based on the length between the leading edge of the flat plate and the center of the cylinder l was more relevant than the usual diameter-based Reynolds number. By changing the velocity of the wind tunnel

the Reynolds number and hence the boundary layer thickness could be varied. Depending on the configuration and the given velocities, the Reynolds numbers ranged from $57,000 \leq Re_l \leq 188,000$ while the relative height was $0.6 \leq h/\delta \leq 2.5$. For all cases the incoming boundary layer was laminar.
In a first approach, a 2D2C-PIV setup was used. The light sheet was positioned vertically through the center of the cylinder in stream wise direction. Two cameras (1280 px x 1024 px) were placed side by side in order to increase the resolution in the stream-wise direction of the 150 mm wide field of view. The particle images were correlated using a multi grid algorithm with image deformation. The final interrogation window size was 32 px x 32 px with an overlap of 75 % and an elliptical weighting function. This resulted in a vector spacing of 0.41 mm. The large pixel shift of up to 25 px was chosen in order to have a good dynamic of the velocity measurement. 500 instantaneous images were recorded per case in order to obtain properly averaged values for velocity, velocity fluctuations, boundary layer thickness and recirculation areas.

Further, a high resolution, large volume 3D3C-PIV setup was used to resolve the unsteady three-dimensional structures in the wake of the cylinder. The beam of two dual-cavity 200 mJ *BigSky* Nd:YAG lasers was expanded and collimated by two telescopes to an elliptical shape that was trimmed by a passe-partout to the final rectangular shape of 70 mm x 8 mm. The beam then was placed parallel to the glass surface, passing 10mm downstream of the cylinder. In order to avoid reflections on the glass, the beam was placed approximately 0.5 mm above the surface. At the end of the glass plate the beam was reflected back into the test section for light enhancement (forward and backward scattering). Four 16 Mpx Imager Pro X cameras equipped with f=105 mm lenses at an aperture of $f_{\#}$=11 were placed in a tetrahedral manner underneath the glass plate, focused on the wake area of the cylinder (Figure 1).

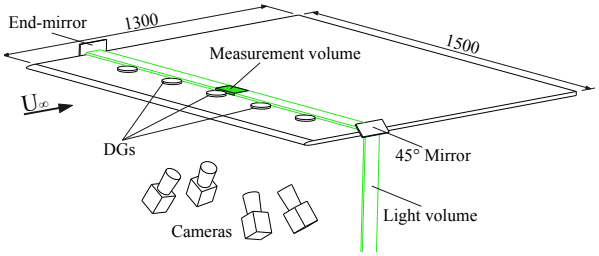

Figure 1: Sketch of the tomographic PIV setup.

For the evaluation of the images, *LaVision's Davis 8* was used. First a volume self calibration was applied [21], where the calibration error was reduced to below 0.2 px. For the reconstruction the MART [3] algorithm was applied on a volume of 67 mm x 91 mm x 8 mm or 2447 x 3324 x 292 voxels. The ghost particle level was below 50 % for all cases. Finally a multigrid correlation with window deformation was performed. Starting with a interrogation window size of 64 px x 64 px x 40 px with an overlap of 50 %, the grid was refined to a final size of 36 px x 36 px x 36 px at an overlap of 75 %, giving a vector density of 66.8 vectors/mm^3 or 3.26 million vectors in the volume. For averaging purposes, 100 double images were recorded for each case. Averaging more than 100 instantaneous vector volumes would be desirable, but the costs for reconstruction and correlation of 100 images were already significant.

3. RESULTS

The analysis of the planar PIV measurements revealed an unexpected behavior of the flow. Unlike at a backward facing step or other 2-dimensional obstacles exposed to a flow, the fluid in the present case does not reattach shortly after the trailing edge, but propagates further into the undisturbed flow as shown in the planar PIV result in figure 2. For the case with the same Reynolds number but a lower $h/\delta = 0.77$ the same effect can be observed although the extent of the vertical disturbance is not as strong as in figure 2.

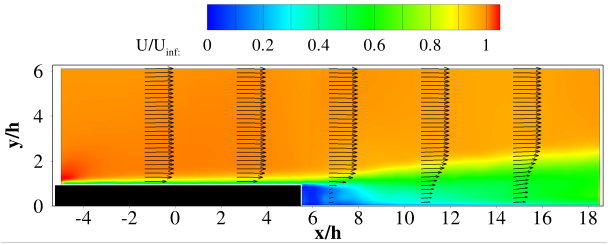

Figure 2: Time averaged velocity magnitude and boundary layer profiles for Re$_l$=108,000 and $h/\delta = 1.75$

The analysis of all cases measured with the 2D2C PIV setup shows that the larger the ratio h/δ, the stronger the wake is influenced. The relative height of the disturbed boundary layer at the downstream location $x/D = 1.6$ over the relative height of the incoming boundary layer is shown in figure 3. h/δ_{wake} denotes the relative height of the boundary layer in the wake of the cylinder, while h/δ_{in} denotes the relative height of the incoming, undisturbed boundary layer.

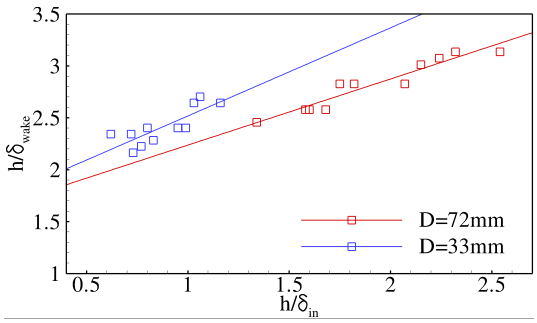

Figure 3: Influence of the incoming boundary layer height h/δ_{in} on the height of the wake h/δ_{wake}

A recirculation area on top of the cylinder as described by Pattenden *et al.* [16] could not be observed in any of the cases. If there is a separation bubble, the height and extension is too small to be captured by the used PIV setup. A small and weak recirculation area that extends about one device height downstream was found directly behind the cylinder. This might be the remainders of the u-shaped arch vortex observed by Pattenden *et al.* for an aspect ratio of 1 where the bow is extending all the way to the surface.

The analysis of the 3D3C-tomographic PIV recordings shed more light into the complex wake behind the cylinder. All cases show a pair of counter-rotating vortices that induce an upward velocity in the center of the wake (Figure 4). This is a significant difference to the observations made by Pattenden *et al.* [16], Sumner *et al.* [19] and others for cylinders with larger aspect ratios. They report two pairs of counter-rotating vortices (base and tip vortex) for aspect ratios larger than three, where the tip vortex has the opposite sense of rotation as in the present case. For aspect ratios between three and one, they observed

the absence of the base vortex. Apparently the sense of rotation of the vortices in the wake changes again for very low aspect ratios. Due to the sense of rotation the present vortices might be related to the base vortices rather than tip vortices as initially thought [19].

These vortices decay in an exponential manner which can be quantified by the averaged circulation distribution in figure 5. The x-vorticity has been integrated over the area around the center of the vortices. There is an uncertainty especially at the upstream part since some part of the vortex extends outside the measurement volume. Here, the magnitude of Γ is underestimated. However, the measurement becomes more reliable towards the downstream end of the volume. It should be noted that one diameter downstream of the cylinder, only 15 % of the initial circulation is left. It was also found that with rising free stream velocity and hence rising h/δ the circulation also increased. This explains the larger wake thicknesses in figure 3.

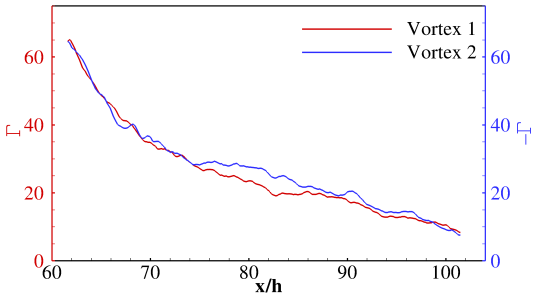

Figure 5: Circulation distribution Γ along the vortex cores for the case Re_l=108,000 and $h/\delta = 1.75$ as in figure 4.

Downstream of the maximum width of the cylinder, two weak vortices can be found. The position and sense of rotation infer that these belong to the horseshoe vortex. It is formed in the corner between the ground and the leading edge of the cylinder when the flow separates. Then it bends around the diameter and propagates into the wake as described by Pattenden [16], Okamoto [14], Marakkos [12] and others.
If h/δ is reduced, the flow around the cylinder is altered. Submerged in the boundary layer, the vortex system becomes more complex as shown in figure 6. The pair of trailing vortices of the previous case is now less dominant and elongated in the cross flow direction.

Further vortices are visible in the flow field downstream of the maximum width of the cylinder. On both sides of the cylinder, a closely spaced pair of counter-rotating vortices could be detected. While the cores of the trailing vortices move closer together as they travel downstream, these vortices keep their distance of about one cylinder diameter. These vortices are located where one usually finds a horseshoe vortex, but the presence of a vortex pair has not been mentioned in most of the literature. Gregory *et al.* [6] observed the presence of several counter-rotating initial horseshoe vortices upstream of a cylinder with aspect ratio Λ=0.5. A smoke visualization for the case where the height of the cylinder is in the order of magnitude of the boundary layer is shown in [20]. However, no propagation of multiple vortices into the wake was reported. Bartkowicz *et al.* [1] found multiple counter-rotating vortices of the horseshoe vortex shed into the wake in their numerical study of the subsonic area upstream of a cylinder in supersonic flow.
In the present case the two vortices downstream of the maximum thickness strongly interact. With higher vortex age, the two vortices rotate and eventually merge, loosing much of the initial individual strength. Finally, only the stronger vortex remains.

Further, the snapshot Proper Orthogonal Decomposition Method (POD) according to Sirovich *et al.* [18] has been applied to 100 instantaneous vector volumes. It was found that the coherent structures in the measurement volume are quite static and hence almost all energy is captured in the mean flow field. The rest of the energy is distributed almost equally over the 100 modes as shown in figure 7. The most energetic mode besides the mean flow contains only 7 times more energy than the least energetic which is a considerably small difference. This observation can be confirmed by looking at the instantaneous vector volumes.

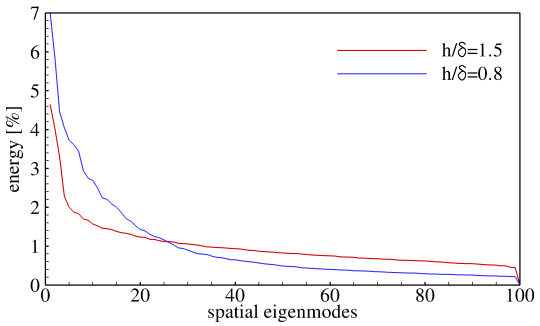

Figure 7: Energy distribution of the POD eigenmodes for $h/\delta = 1.75$ and $h/\delta = 0.8$

In the turbulent wake behind the cylinder, it is difficult to extract clear flow features in the instantaneous flow fields. Therefore the flow field was reconstructed using only the 10 most energetic eigenmodes of the POD (Low Mode Reconstruction, LOM). With such an approach, vortical structures and their dominant sense of rotation could be filtered from non-coherent structures, such as turbulence and noise. A result of the LOM is shown in figure 8 for the case with $h/\delta = 0.8$, Re_l=108,000.

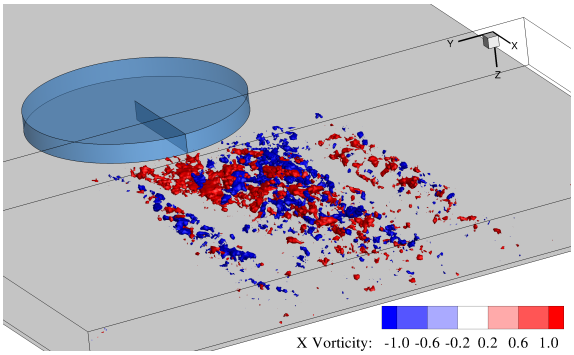

Figure 8: LOM reconstruction of an instantaneous vector volume with 10 POD modes for the case $h/\delta = 0.8$, Re_l=108,000. Iso-surfaces of x-vorticity.

4. CONCLUSIONS

The wake of a wall mounted cylinder with an aspect ratio of as little as Λ=0.09 has been investigated by means of planar and high resolution tomographic PIV. Four 16Mpx CCD cameras were used to record particles illuminated by two coupled pulsed lasers. The non-dimensional initial boundary layer thickness was $0.6 \leq h/\delta \leq 2.5$, depending on the model and the Reynolds number Re_l used. The results of the planar PIV show upward flow in the symmetry plane, increasing the height of the wake

for all cases. With a decreasing boundary layer thickness, the influence on the wake increases. The results of the tomographic PIV revealed a pair of counter-rotating vortices in the wake of the cylinder that induces a positive normal velocity. The circulation of these vortices increases with increased Reynolds number and hence h/δ. If the cylinder was further submerged into the boundary layer, the vortex system became more complex: The trailing vortices are pinched and a horseshoe-like vortex pair on both sides of the cylinder interacts along the measurement volume. For all configurations the vortices decay quickly due to interactions with the boundary layer and lost the major part of the circulation already one diameter downstream. The trailing vortices which induce an upward facing velocity and hence increase the wake height might explain the large effect of these small low aspect ratio cylinders (LEVoGs) while mounted onto a pitching airfoil.

Further configurations where the wake of the cylinder is exposed to an instability are subject of the current work.

ACKNOWLEDGMENTS

The present work has been performed in cooperation with the department of experimental methods of the DLR Göttingen. The authors also acknowledge the support of LaVision GmbH.

REFERENCES

[1] M.D. Bartkowicz and P.K. Subbareddy. Numerical simulation of roughness induced instability in the purdue mach 6 wind tunnel. *AIAA Paper*, (2010-4723), 2010.

[2] L.W. Carr. Analysis of the development of dynamic stall based on oscillating airfoil experiments. *NASA TN-8382*, 1977.

[3] G. Elsinga, F. Scarano, B. Wieneke, and B. van Oudheusden. Tomographic particle image velocimetry. *Experiments in Fluids*, 41:933–947, 2006.

[4] T. A. Fox and G. S. West. Fluid-induced loading of cantilevered circular cylinders in a low-turbulence uniform flow. part 1: Mean loading with aspect ratios in the range 4 to 30. *Journal of Fluids and Structures*, 7(1):1 – 14, 1993.

[5] W. Geissler, G. Dietz, H. Mai, J. Bosbach, and Richard H. Dynamic stall and its passive control investigations on the oa209 airfoil section. *31. European Rotorcraft Forum*, 2005.

[6] N. Gregory and W.S: Walker. The effect on transition of isolated surface excrescences in the boundary layer. *Aeronautical Research Council R & M*, (2779), 1956.

[7] B. Heine, K. Mulleners, and A. Gardner. On the effects of leading edge vortex generators on an oa209 airfoil. *10th ONERA-DLR Aerospace Symposium ODAS Berlin*, 2009.

[8] B. Heine, T. Schwermer, and M. Raffel. The effect of vortex generators on the flow around a circular cylinder. *15th Int Symp on Applications of Laser Techniques to Fluid Mechanics, Lisbon*, 2010.

[9] T. Kawamura, M. Hiwada, T. Hibino, I. Mabuchi, and M. Kumada. Vortex shedding from a circular cylinder of finite length placed on a ground plane. *Bulletin of JSME*, 27(232):2142–2151, 1984.

[10] L.W. Lee and Y.L. Wang. Aerodynamics of a circular cylinder of finite length in cross-flow. *Proceedings of the ASME Applied Mechanics, Bioengineering, and Fluids Engineering Conference*, pages 61–65, 1987.

[11] H. Mai, G. Dietz, W. Geissler, K. Richter, J. Bosbach, H. Richard, and K. de Groot. Dynamic stall control by leading edge vortex generators. *American Helicopter Society*, 62, 2006.

[12] Konstantinos Marakkos and John T. Turner. Vortex generation in the cross-flow around a cylinder attached to an end-wall. *Optics & Laser Technology*, 38(4-6):277 – 285, 2006.

[13] W.J. McCroskey. The Phenomenon of Dynamic Stall. *NASA TM-81264*, 1981.

[14] Shiki Okamoto and Yukisada Sunabashiri. Vortex shedding from a circular cylinder of finite length placed on a ground plane. *Journal of Fluids Engineering*, 114(4):512–521, 1992.

[15] Cheol-Woo Park and Sang-Joon Lee. Free end effects on the near wake flow structure behind a finite circular cylinder. *Journal of Wind Engineering and Industrial Aerodynamics*, 88(2-3):231 – 246, 2000.

[16] R. J. Pattenden, S. R. Turnock, and X. Zhang. Measurements of the flow over a low-aspect-ratio cylinder mounted on a ground plane. *Experiments in Fluids*, 39:10–21, 2005.

[17] Hiroshi Sakamoto and Mikio Arie. Vortex shedding from a rectangular prism and a circular cylinder placed vertically in a turbulent boundary layer. *Journal of Fluid Mechanics*, 126:147–165, 1983.

[18] L. Sirovich. Turbulence and the dynamics of coherent structures part1: Coherent structures. *Quarterly of Applied Mathematics*, 45(3):561–571, 1987.

[19] D. Sumner, J. L. Heseltine, and O. J. P. Dansereau. Wake structure of a finite circular cylinder of small aspect ratio. *Experiments in Fluids*, 37:720–730, 2004.

[20] Bryan. Thwaites. *Incompressible aerodynamics : an account of the theory and observation of the steady flow of incompressible fluid past aerofoils, wings, and other bodies*. Clarendon Press, Oxford :, 1960.

[21] B. Wieneke. Volume self-calibration for 3d particle image velocimetry. *Experiments in Fluids*, 45:549–556, 2008.

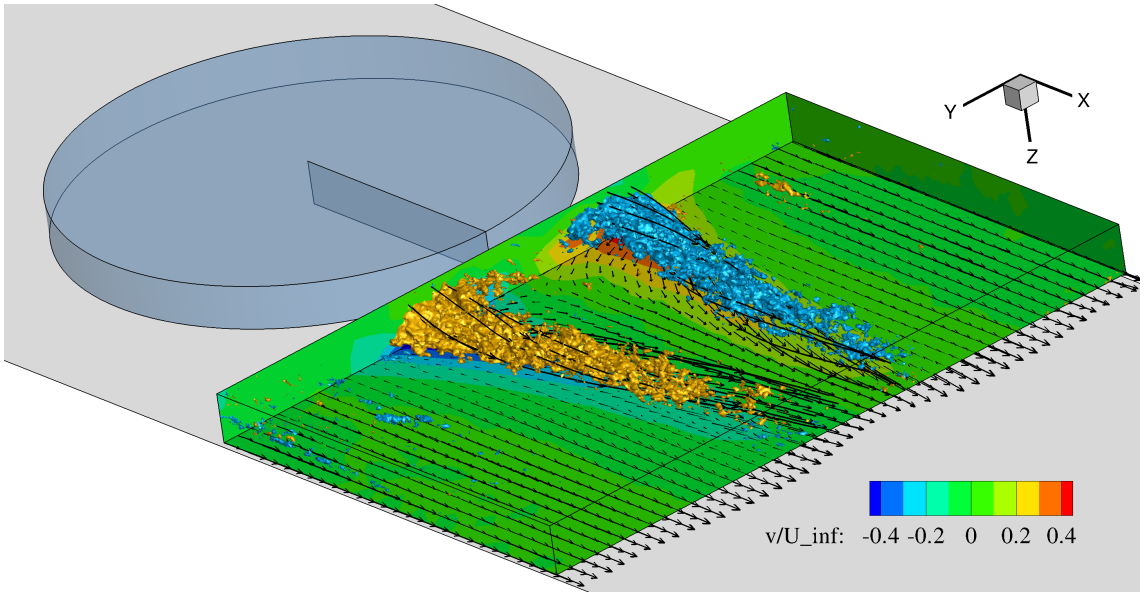

Figure 4: Time-averaged wake behind the low aspect ratio cylinder for the case $h/\delta = 1.75$, Re_l=108,000. Iso-surfaces of helicity ($H_n = \pm 2$), v-velocity coded contours and streamlines.

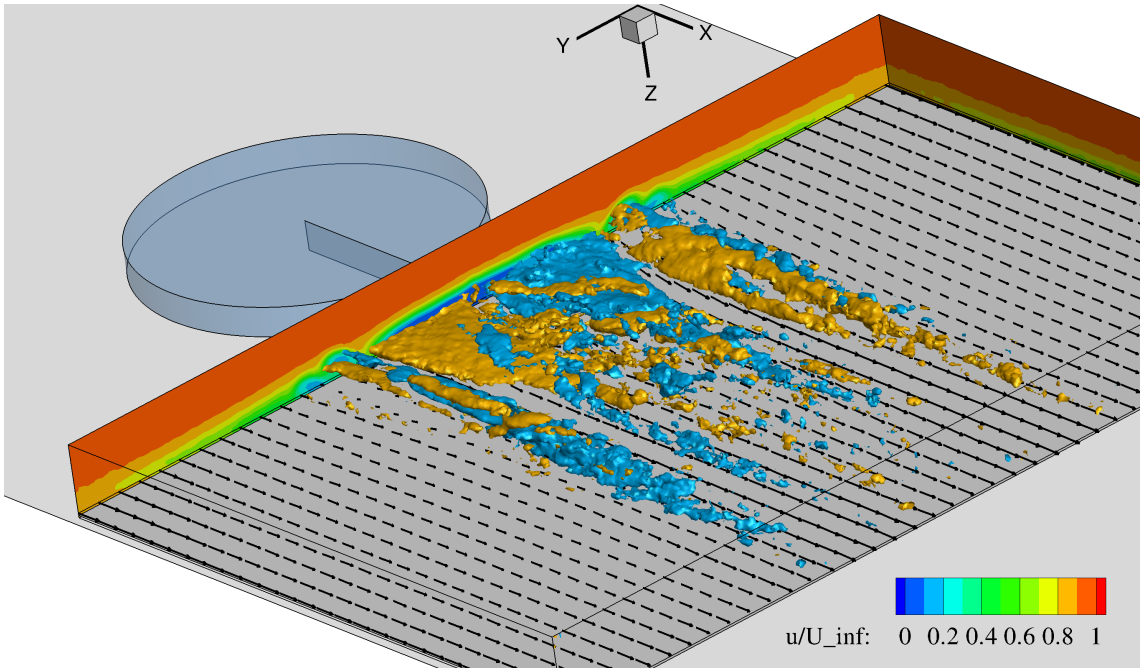

Figure 6: Time-averaged wake behind the low aspect ratio cylinder for the case $h/\delta = 0.8$, Re_l=108,000. Iso-surfaces of x-vorticity ($\xi_x = \pm 0.4$) and velocity magnitude coded contours.